JACS
JOURNAL OF THE AMERICAN CHEMICAL SOCIETY
Article
pubs.acs.org/JACS

Ultrahigh Surface Area Zirconium MOFs and Insights into the Applicability of the BET Theory

Timothy C. Wang,[†,⊥] Wojciech Bury,[†,§,⊥] Diego A. Gómez-Gualdrón,[‡] Nicolaas A. Vermeulen,[†] Joseph E. Mondloch,[†] Pravas Deria,[†] Kainan Zhang,[†] Peyman Z. Moghadam,[‡] Amy A. Sarjeant,[†] Randall Q. Snurr,*[,‡] J. Fraser Stoddart,*[,†] Joseph T. Hupp,*[,†] and Omar K. Farha*[,†,∥]

[†]Department of Chemistry and [‡]Department of Chemical and Biological Engineering, Northwestern University, Evanston, Illinois 60208, United States

[§]Department of Chemistry, Warsaw University of Technology, Noakowskiego 3, 00-664 Warsaw, Poland

[∥]Department of Chemistry, Faculty of Science, King Abdulaziz University, Jeddah 22254, Saudi Arabia

Supporting Information

ABSTRACT: An isoreticular series of metal−organic frameworks (MOFs) with the **ftw** topology based on zirconium oxoclusters and tetracarboxylate linkers with a planar core (**NU-1101** through **NU-1104**) has been synthesized employing a linker expansion approach. In this series, **NU-1103** has a pore volume of 2.91 cc g^{-1} and a geometrically calculated surface area of 5646 m^2 g^{-1}, which is the highest value reported to date for a zirconium-based MOF and among the largest that have been reported for any porous material. Successful activation of the MOFs was proven based on the agreement of pore volumes and BET areas obtained from simulated and experimental isotherms. Critical for practical applications, **NU-1103** combines for the first time ultrahigh surface area and water stability, where this material retained complete structural integrity after soaking in water. Pressure range selection for the BET calculations on these materials was guided by the four so-called "consistency criteria". The experimental BET area of **NU-1103** was 6550 m^2 g^{-1}. Insights obtained from molecular simulation suggest that, as a consequence of pore-filling contamination, the BET method overestimates the monolayer loading of **NU-1103** by ∼16%.

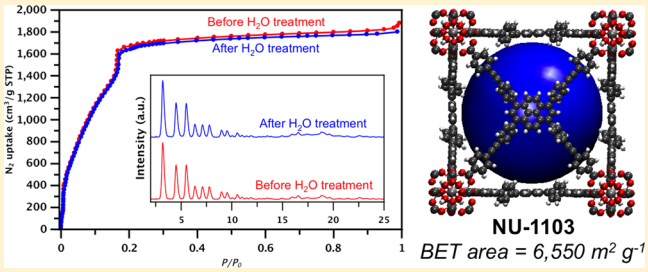

1. INTRODUCTION

Metal−organic frameworks (MOFs) are a class of crystalline materials formed by coordination bonds between metal-based nodes and organic linkers.[1−3] By judicious choice of building blocks, MOFs with many desirable physical properties have been synthesized. Some of the most desirable characteristics of MOFs are their permanent porosity and ultrahigh (Brunauer−Emmett−Teller (BET) ≥ 6000 m^2 g^{-1}) specific surface areas. The realization of ultrahigh surface areas within MOFs has, in turn, pushed the limit of practical sorption based gas storage technologies, e.g., molecular hydrogen and natural gas.[4−7] Indeed, Toyota will start selling hydrogen fueled vehicles in California in early 2015.[8] Forward looking, Mercedes Benz is pursuing the use of MOFs in hydrogen storage systems for next generation fuel cell vehicles.[9]

The synthesis of ultrahigh surface area MOFs has been advanced largely by utilizing the concept of "isoreticular expansion", the expansion of organic linker length in a given MOF topology.[10] Some of the highest known surface area MOFs, including **MOF-210**,[5] **NU-100**,[4] **NU-109**,[6] **NU-110**,[6] **DUT-32**,[7] and **DUT-49**,[11] have been synthesized using this strategy and have registered specific surface areas as high as 7140 m^2 g^{-1} (**NU-110**), as determined by applying BET theory to measured nitrogen isotherms. While isoreticular expansion may appear deceptively simple, several potential pitfalls still need to be circumvented en route to ultrahigh surface area materials.[12,13] For instance, linker expansion engenders a tendency for MOFs to collapse upon solvent removal. Gentle supercritical CO_2 activation, a technique developed at Northwestern University, has been shown useful, however, in addressing this issue.[14−17] Although long linkers may also lead to the formation of interpenetrated structures, synthesizing MOFs in topological nets that are not prone to interpenetration can alleviate this tendency. In fact, this rationale was used in the synthesis of **NU-110**[6] and **DUT-32**,[7] which are based, respectively, on the **rht** and **umt** topologies that inherently forbid interpenetration.

One key limitation in exploiting ultrahigh surface area in practical applications of MOFs has been their lack of water (or moisture) stability. For example, it is often advantageous for materials to be stable toward oxygen and moisture during material processing (e.g., pellet formation). To date, ultrahigh surface area MOFs have been based exclusively on Zn_4O or Cu_2

Received: December 21, 2014
Published: February 27, 2015

DOI: 10.1021/ja512973b
J. Am. Chem. Soc. 2015, 137, 3585−3591

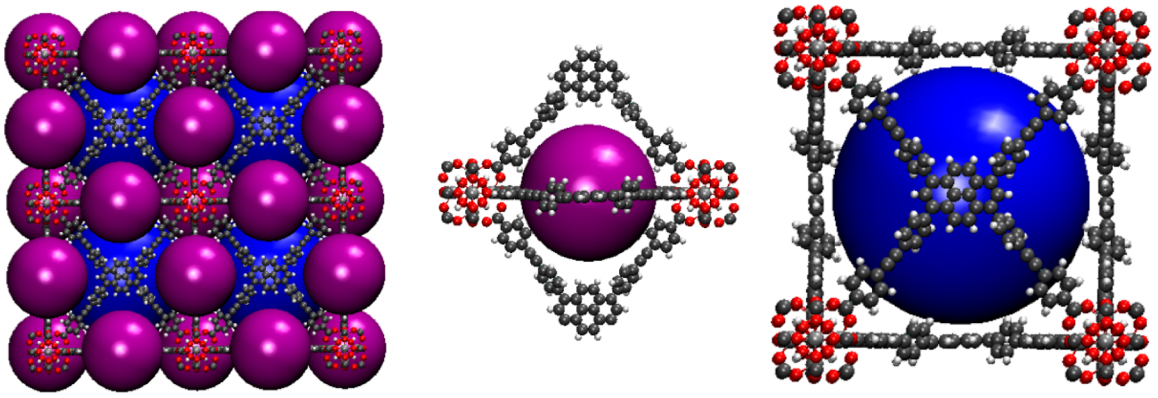

Figure 1. Structural features of the **ftw** topology illustrated in **NU-1103** with large pores (indicated with blue spheres) located at the center of the cubic unit cell and small pores (indicated as purple spheres) located at the edges of the cubic unit cell.

metal-based clusters with linkers containing carboxylate groups, which unfortunately lose crystallinity and surface area when exposed to moisture.[18] Herein, we utilize the isoreticular expansion approach to synthesize a series of water stable zirconium-oxo/hydroxo cluster-based MOFs, **NU-1101** through **NU-1104**, based on the **ftw** topology. One of these MOFs, **NU-1103**, which has a geometric surface area of 5646 $m^2\ g^{-1}$ (and BET area of 6550 $m^2\ g^{-1}$), exhibits the highest geometric surface area (and BET area) reported for any zirconium oxocluster containing MOF.

2. EXPERIMENTAL SECTION

All air- or water-sensitive reactions were carried out under a dry nitrogen atmosphere using Schlenk techniques. Chemicals were purchased from Oakwood Products, Inc. (West Columbia, SC), Strem Chemicals (Newburyport, MA), and Aldrich Chemicals Co. (Milwaukee, WI) and used without further purification. All gases used for adsorption and desorption measurements were ultrahigh purity grade 5 and were obtained from Airgas Specialty Gases (Chicago, IL).

Synthesis of NU-1101. $ZrOCl_2{\cdot}8H_2O$ (96 mg, 0.30 mmol) and benzoic acid (2.7 g, 22 mmol) were mixed in DMF (8 mL in a 6-dram vial) and sonicated until the solid dissolved. The clear solution was incubated in an oven at 80 °C for 1 h. After cooling down to room temperature, **Py-XP** (66 mg, 0.06 mmol) was added to this solution, and the mixture was sonicated for 10 min. The colorless solution was heated in an oven at 120 °C for 48 h. After cooling down to room temperature, colorless cubic-shaped crystals were isolated by filtration and washed with fresh DMF.

Synthesis of NU-1102. In an O_2 and H_2O free drybox, $ZrCl_4$ (37.5 mg, 0.16 mmol) was weighed into a 4-dram vial. The vial was removed from the glovebox, and **Por-PP** (59 mg, 0.054 mmol) along with 4 mL DEF was added into the vial. The solution was sonicated until green homogeneous slurry was obtained. Next, benzoic acid (675 mg, 5.5 mmol) was added into the slurry and sonicated until dissolved. Finally, the 4-dram vial was sealed and placed in an oven at 120 °C for 3 days. After 3 days, dark purple crystals were formed on the walls and bottom of the vials, and the mother liquor was removed.

Synthesis of NU-1103. In an ambient condition, **Py-PTP** (25 mg, 0.023 mmol) and benzoic acid (1 g, 8.92 mmol) were added into a 6-dram vial. Twenty mL of DMF is then added, and the vial was sonicated to fully dissolve the reagents. Then, $ZrOCl_2{\cdot}8H_2O$ (10 mg, 0.03 mmol) was quickly weighed into the vial containing the reagents, and the vial was sonicated again until no solid could be found in the vial. The solution prepared was divided into two portions, which is achieved by transferring half of the solution into an empty 6-dram vial by pipet. The two vials prepared were heated in a heating block on a hot plate, and the temperature of the heating block is set at 120 °C by using thermocouple. After 24 h, vials were taken out from the heating block, and the mother solution was removed by centrifuging (10 min, 7000 rpm).

Synthesis of NU-1104. $ZrOCl_2{\cdot}8H_2O$ (16 mg, 0.05 mmol) and benzoic acid (600 mg, 4.9 mmol) of were mixed in 8 mL of DMF (in a 6-dram vial) and sonicated until the solid dissolved. The clear solution was incubated in an oven at 80 °C for 1 h. After cooling down to room temperature, **Por-PTP** (12 mg, 0.01 mmol) was added to this solution, and the resulting mixture was sonicated for 10 min. The dark purple solution was heated in an oven at 120 °C for 48 h. After cooling down to room temperature, dark purple cubic-shaped crystals were separated from amorphous phase by centrifuging in DMF. Approximately 25 mg of solvated crystalline material was placed in a 4-dram vial with 3 mL of DMF. Then a solution of 30 mg of $NiCl_2{\cdot}H_2O$ in DMF (1 mL) was added, and the vial was swirled gently and placed in an oven at 90 °C for 2 days to metalate the porphyrin core.

3. RESULTS AND DISCUSSION

Presynthesis Design. In an attempt to address the issue of moisture and water stability we decided to pursue MOFs based on zirconium-oxoclusters and carboxylate-based linkers. Water stable MOFs based on other building units have been reported in the literature,[19,20] but they are not suitable to reach ultrahigh surface areas.[21] Zirconium-oxocluster MOFs[22−24] have been shown to exhibit general stability toward water and acid as well as a wide range of organic solvents.[24−33] The remarkable stability of zirconium-based MOFs is driven by the strong bonding between zirconium ions and carboxylate oxygens present in the linkers. On account of the high molecular weight of the Zr-oxoclusters (vs Cu_2 or Zn_4O based nodes), it might seem counterintuitive to pursue ultrahigh surface areas materials with Zr-based MOFs. It is notable that the highest surface area (as calculated by BET theory) reported[28,34] to-date for Zr-oxocluster-based MOFs is ∼4500 $m^2\ g^{-1}$.

Recently, however, through calculation of geometric surface areas, Gomez-Gualdron et al.[35] demonstrated that ultrahigh surface areas are achievable for Zr-based MOFs with reasonable expansion of tetratopic linkers with (nearly) square-planar symmetry in the **csq**, **scu**, or **ftw** topologies, wherein the **ftw** topology (Figure 1) shows the highest potential surface area. Initial calculations (see Supporting Information (SI) for additional details) also indicated that the **ftw** topology minimizes the propensity for catenation. Zirconium-based MOFs with this topology are based on a cubic unit cell with zirconium oxoclusters at the vertices connected by planar tetratopic linkers across the faces. The zirconium nodes have the same structure as the well-known **UiO-66**.[22] Although the **ftw** topology has been depicted[28,36] as a collection of cubic

DOI: 10.1021/ja512973b
J. Am. Chem. Soc. 2015, 137, 3585−3591

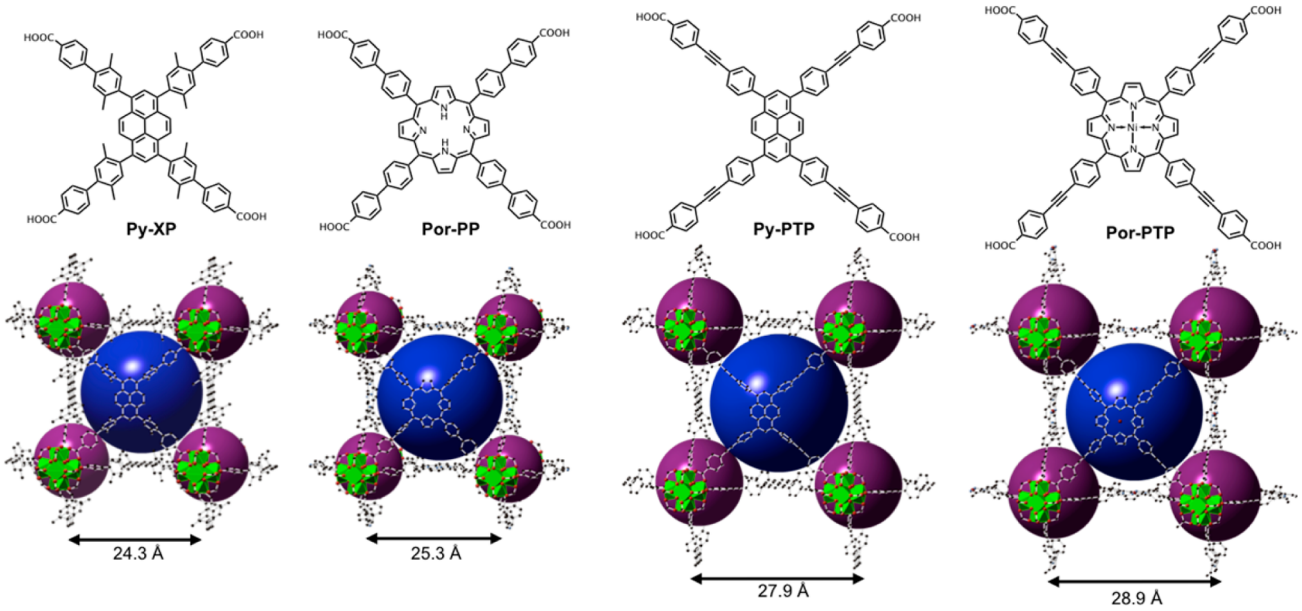

Figure 2. Tetratopic organic linkers (**Py-XP**, **Por-PP**, **Py-PTP**, **Por-PTP**) used and the crystal structures of **NU-1101** to **NU-1104**. The increasing dimensions of the organic linkers result in the reticular expansion of the MOF structure, with unit cell parameters of the cubic cells being 24.3, 25.3, 27.9, and 28.7 Å, respectively. Two-thirds of the small cavities (purple spheres) were neglected for clarity when showing the unit cells of **NU-110x** series. The calculated pore diameter for **NU-110x** series: **NU-110x** (dl, ds) = NU-1101 (17.2, 9.5), NU-1102 (20.5, 11.1), NU-1103 (22.7, 12.7), NU-1104 (24.2, 13.5). dl = large pore diameter, ds = small pore diameter. All units are in Å.

cages, Figure 1 shows that this topology features two types of pores: (1) large pores (indicated with blue spheres) located at the center of the cubic unit cell and (2) small pores (indicated as purple spheres) located at the edges of the cubic unit cell.

Our selection of tetratopic linkers was based on the *in silico* evaluation of geometric surface areas of MOFs with the **ftw** topology and **Py-XP**, **Por-PP**, **Py-PTP**, and **Por-PTP** as the linkers. This combination results in an isoreticular series of MOFs which we have termed **NU-1101** through **NU-1104** (Figure 2).

It is noteworthy that inconsistencies in the application of the consistency criteria,[37] for comparison of materials based on their reported BET areas, may be problematic for these and other materials with ultrahigh surface areas.[7] In order to circumvent this issue and benchmark target materials properly, we have calculated surface areas geometrically using a rolling-probe method, which is independent of the nitrogen isotherm and the BET theory.[38] The calculated geometric surface areas for **NU-1101** through **NU-1104** are shown in Table 1, along with the calculated geometric surface areas for other ultrahigh surface area MOFs. Somewhat pleasingly, **NU-1103** exhibits a calculated geometric surface area of 5646 $m^2\ g^{-1}$, a value which is only 10% lower than the current record holder (**NU-110**).

Synthesis and Experimental Characterization. In light of the computational results, the candidate tetratopic organic linkers, **Py-XP**, **Por-PP**, **Py-PTP**, and **Por-PTP**, were synthesized by Sonogashira or Suzuki coupling, followed by saponification in basic aqueous solution (see SI for details).

Solvothermal reactions between zirconium salts and each linker in DMF at elevated temperature all afforded cubic crystals, and the crystal structures were determined by single crystal X-ray diffraction (see SI), and as anticipated, each structure shows cubic symmetry and adopts the **ftw** topology, with no interpenetration of the structure. All MOFs in the **NU-110x** series showed excellent agreement between the simulated

Table 1. Summary of Calculated Geometric Surface Areas for Ultrahigh Surface Area MOFs

MOF	geometric surface area ($m^2\ g^{-1}$)	ref
NU-110	6229	6
NU-109	6175	6
NU-100	5822	4
MOF-210	5770	5
NU-1103	**5646**	**this work**
DUT-32	5297	7
NU-1104	**5290**	**this work**
DUT-49	5176	10
NU-1102	**4712**	**this work**
MOF-177	4673	5
NU-1101	**4422**	**this work**
NU-1100	3892	23
MOF-5	3434	34

(Figure 3) and measured powder X-ray diffraction (PXRD) patterns, demonstrating the bulk purity of the materials.

The thermal stability of **NU-1101** through **NU-1104** was assessed by thermogravimetric analysis (TGA). The results revealed that all the materials are stable at elevated temperature, having decomposition temperatures around 470 °C (see SI section S8.). The TGA of the solvated samples all show significant weight loss due to guest solvent molecules in the cavity prior to 200 °C, consistent with the highly porous nature of these materials.

An important consideration when working with ultrahigh surface area MOFs is the removal of solvent molecules from the pores of the crystals while leaving the framework pores intact and accessible.[16] On moving from DMF to acetone,[40] a lower boiling point solvent, followed by heating under dynamic vacuum, **NU-1101** and **NU-1102** could both be activated, as evidenced by the PXRD patterns (SI Figures S7.1 and S7.2) as well as by the N_2 adsorption isotherm (Figure 4a). When a

DOI: 10.1021/ja512973b
J. Am. Chem. Soc. 2015, 137, 3585−3591

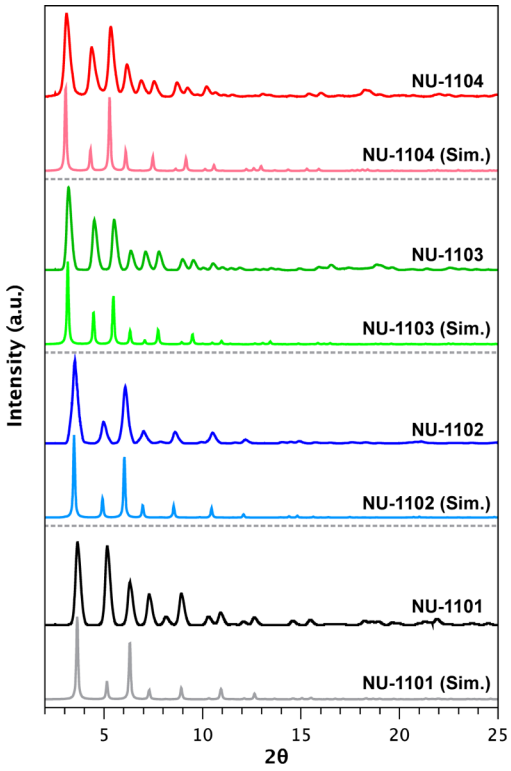

Figure 3. PXRD of the as-synthesized MOFs. The agreement between the simulated and measured diffraction patterns indicates the phase purity of the bulk material.[39]

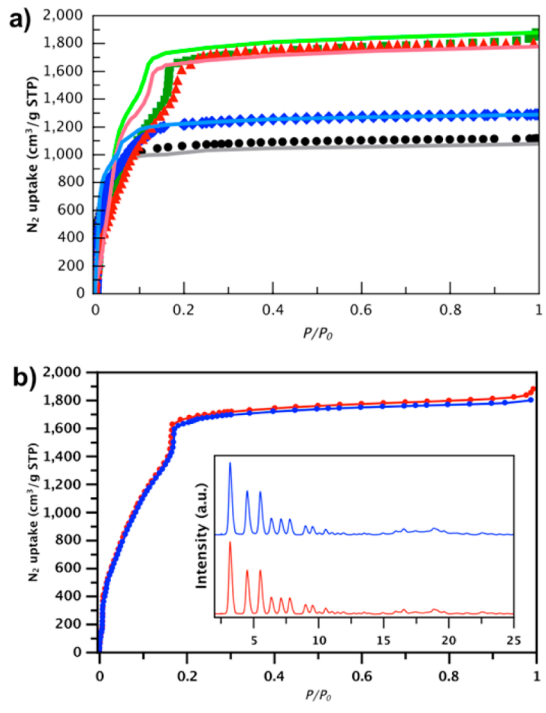

Figure 4. (a) Nitrogen isotherms for **NU-1101** through **NU-1104** (solid lines: simulated isotherm; symbols: experimental isotherm; black: **NU-1101**, blue: **NU-1102**, green: **NU-1103**, red: **NU-1104**). (b) PXRD patterns (inset) and nitrogen isotherms remained identical before and after water treatment (blue: reactivated sample after soaking in water, red: **NU-1103** right after activation step).

similar procedure was used with **NU-1103** and **NU-1104**, however, their crystallinity was lost, and the resulting materials exhibited little porosity. In order to activate **NU-1103** and **NU-1104** fully, supercritical CO_2 drying[14] was utilized so as to avoid capillary forces collapsing the MOFs. Under these conditions, both **NU-1103** and **NU-1104** retained their crystallinity (SI Figures S7.3 and S7.4) and porosity (Figure 4a) upon activation.

Nitrogen isotherms were measured (Figure. 4a) at 77 K for **NU-1101** through **NU-1104** to assess their porosities and surface areas (*vide infra*). The pore volumes extracted from the nitrogen saturation loadings measured for all samples agree very well with those extracted from nitrogen isotherms simulated by Grand Canonical Monte Carlo (GCMC) simulations (see SI section 9). Indeed, the agreement between measured and simulated nitrogen isotherms indicates the successful nature of the activation and suggests that essentially all of the calculated geometric surface area should be accessible.

The porosity of the **NU-110x** series rises as the linker length increases, and the observed pore volumes are 1.72, 2.00, 2.91, and 2.79 cc g^{-1} for **NU-1101**, **NU-1102**, **NU-1103**, and **NU-1104**, respectively. The pore size distribution, calculated from nitrogen isotherms with the BJH desorption model, also agrees well with the simulated data. Each MOF showed two types of pores, which were anticipated from the crystal structures, i.e., a larger pore centered at (1/2,1/2,1/2) and a smaller centered at (1/2,0,0). Similar to the pore volume, the pore sizes also become larger with increasing linker length. The size of the larger pore was found to increase from 17.2 to 24.2 Å throughout the series, while the size of the smaller pore is 9.5–13.5 Å. These pore sizes range from microporous (<20 Å) to mesoporous (≥20 Å) and are consistent with the observed steps in the N_2 isotherms of **NU-1103** and **NU-1104**.

In order to demonstrate the water stability of the ultrahigh surface area Zr-oxocluster-based MOFs, we selected the material with the largest geometric surface area in the series, namely **NU-1103**, and soaked it in water at room temperature for 18 h. Given the propensity toward capillary force-driven collapse when activated from water,[24] the solvent was then changed to ethanol. Subsequent supercritical CO_2 drying resulted in the activated MOF. Remarkably, the nitrogen isotherm and PXRD pattern measured for this water-treated sample were identical (Figure 4b) to those measured before treatment. This full retention of porosity demonstrates that the material is water-stable under the conditions tested.

Calculation of the BET Area and Discussion of the Applicability of BET Theory. Since the PXRD and sorption measurements suggested excellent agreement between the simulated and synthesized structures, it is reasonable to assume that the members of the **NU-110x** series possess the calculated geometric surface areas listed in Table 1, with **NU-1103** registering the highest one among these zirconium-based MOFs. To obtain experimental estimates for N_2-accessible surface areas, the BET analysis of nitrogen isotherms is commonly employed. Although several assumptions made in BET theory may not apply rigorously to MOFs, the theory has still been a valuable predictor of relative gas-storage performance for members of a related series MOFs.[41]

The BET equation:

$$\frac{p/p_0}{n(1-p/p_0)} = \frac{1}{n_m C} + \frac{C-1}{n_m C}(p/p_0)$$

DOI: 10.1021/ja512973b
J. Am. Chem. Soc. 2015, 137, 3585–3591

is derived[42] from the assumptions of BET theory and has been commonly used to get an experimental value of the surface area of a material by plotting the left-side of the equation as a function of p/p_0. From such a plot, a linear region is identified. From the fitted slope $((C-1)/n_mC)$ and intercept $(1/n_mC)$, the value of the monolayer capacity n_m and the BET constant C can be extracted. A critical step, therefore, in the determination of the BET area is to select the "correct" linear pressure range, as the value of the BET area obtained can be greatly affected by this choice. Indeed, there may appear more than one linear range to select from, and thus application of consistency criteria, as suggested by Rouquerol et al.,[43] is recommended to guide the selection of the appropriate pressure range.

Briefly, the consistency criteria state that (1) Only a range where $n(1-p/p_0)$ increases monotonically with p/p_0 should be selected; (2) the value of the BET constant C, resulting from the linear fit, should be positive; (3) the monolayer loading n_m should correspond to a pressure in the selected range; (4) the calculated value for monolayer formation $(1/(\sqrt{C}+1))$, should be equal to the pressure determined in criterion 3. We used these criteria to select the pressure ranges in the measured and simulated nitrogen isotherms of the **NU-110x** series[44] to be able to consistently compare experimental and simulated BET area values. Detailed BET calculations and discussion of the consistency criteria are reported in the SI.

We discovered that, while the application of the first and second consistency criteria was straightforward, the application of the third and fourth criteria was often fraught with problems. For all structures, a tolerance of around 10% was needed to satisfy the third consistency criterion, which requires the pressure corresponding to monolayer formation to be within the chosen pressure range. For instance, for **NU-1103**, the selected pressure range for calculating the BET area was $0.036 < p/p_0 < 0.164$, although the p/p_0 value corresponding to monolayer capacity n_m was 0.169, which is 3.0% above the upper pressure limit. Indeed, the use of reasonable tolerances may be needed to account for small deviations relating to some of the BET assumptions. In fact, a similar tolerance has been proposed by Rouquerol et al.[43] for the fourth criterion, where a 20% tolerance for the relation that $(p/p_0)_m = 1/(\sqrt{C}+1)$ is suggested.

Similar deviations from the consistency criteria were observed when applying BET calculations to simulated isotherms, with similar tolerances needed to satisfy the criteria. Therefore, to calculate an apparent BET area[44] for each of these materials, we chose the pressure range that satisfied the largest number of criteria and minimized the error for any criterion not satisfied (see SI Table S9.1). From the measured (simulated) isotherms we obtained BET areas of 4340 (4350), 4830 (4730), 6550 (6860), and 6230 (6262) $m^2\ g^{-1}$. Notice that the application of the consistency criteria as guidelines to select the pressure range for BET calculation allowed a consistent comparison between measured and simulated values. On these grounds, the agreement of the BET areas obtained from simulated versus measured isotherms (in addition to pore volumes and PXRDs) indicates the successful activation of the materials and further confirms that it is possible to achieve ultrahigh surface areas in water-stable zirconium-based MOFs, as demonstrated by the isoreticular expansion in the **NU-110x** series.

Given the importance of the BET method for experimental characterization of MOFs, and taking advantage of the fact that an isoreticular series of structures was synthesized and completely activated, we decided to analyze the molecular configurations from the simulated nitrogen isotherms to gain insights into deviations from the BET theory in structures with different pore sizes and the discrepancy between BET areas and geometric surface areas of some members of the **NU-110x** series. Using a simple automated algorithm, for each structure and selected pressure, we counted the total number of nitrogen molecules (blue line in Figure 5) in the cubic unit cell and identified those in contact with the pore walls with a tolerance of 1.0 Å (pink line in Figure 5), which represent the formation of the monolayer.

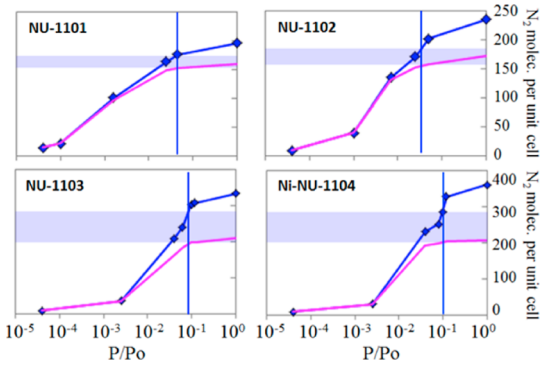

Figure 5. Simulated N_2 isotherm (blue) and the number of molecules in monolayer contact (pink). The vertical blue line is the pressure corresponding to the monolayer formation as determined by BET calculations, and the shaded blue area indicates the amount of adsorbed N_2 that is not forming the monolayer in the simulation but is counted toward the monolayer in the BET analysis.

Notice that at low pressures, all of the nitrogen is adsorbed on the walls, thus contributing to the monolayer formation. As the pressure is increased beyond a structure-dependent value, pore filling starts to occur while the "monolayer" is still being formed. The vertical line indicates the pressure predicted to correspond to the monolayer formation from the BET calculation using the simulated isotherms. Intriguingly, this pressure, $(p/p_0)_m$, seems to be a good indication of when the monolayer is essentially complete (i.e., the number of molecules contacting the pore walls reaches saturation), as indicated by the pink curves reaching a plateau after this specific pressure. The degree of pore filling "contamination" of the BET estimates of monolayer loading at $(p/p_0)_m$ is largest for **NU-1103** and **NU-1104**, materials whose porosities place them in the transition range between microporosity and mesoporosity. We hypothesize that this pore filling contamination contributes to the consistency criteria not being rigorously fulfilled, and it evidently contributes to overestimation of the monolayer loading. This phenomenon seems to generally occur in other structures with pores in the transition range between microporosity and mesoporosity, and it will be thoroughly investigated for a comprehensive set of structures in upcoming work.

4. CONCLUSIONS

We found that by employing hexa-zirconium oxo/hydroxo nodes and tetra-carboxylated linkers, water-stable MOFs featuring the noncatenating **ftw** topology and characterized by ultrahigh surface areas, can be synthesized and fully activated. To our knowledge, all previous experimental forays into the realm of ultrahigh surface area MOF chemistry,

DOI: 10.1021/ja512973b
J. Am. Chem. Soc. 2015, 137, 3585−3591

including our own, have been plagued, from an applications perspective, by sensitivity of the activated versions of the materials to water vapor (i.e., degradation by water).

Each of the MOFs examined here features a pair of pore types, which is signaled in N_2 adsorption isotherms by a sharp and sizable step at a p/p_0 value between 0.1 and 0.2. From GCMC simulations, the physical significance of the unusual isotherm shape includes in some instances somewhat significant pore filling before monolayer coverage of the surfaces of both pores is achieved, which leads the BET theory to overestimate the monolayer coverage. In turn, this finding suggests that the Rouquerol consistency criteria for data-range selection for accurate application of the BET analysis may be impossible to satisfy. Indeed, we find that to varying degrees this is the case. A practical consequence, that will be explored in quantitative detail elsewhere, is that BET areas may exceed true N_2-accessible surface areas for these complex materials by up to several hundred $m^2\ g^{-1}$ (i.e., up to ~15%).[45] Nevertheless, the analysis returns reliable *relative* surface areas for the series of compounds examined. Notice that if experimental BET areas are to be used to assess the activation of a MOF, comparison to BET areas from simulated N_2 isotherms is more reliable than comparison to geometrically calculated areas.

With 5646 m^2g^{-1}, **NU-1103** possesses the highest geometric surface area (and a BET area of 6550 $m^2\ g^{-1}$) yet reported for a water-stable MOF. This record-breaking property renders **NU-1103** attractive for practical applications such as hydrogen storage, as it simultaneously addresses the well-known need for high capacity and the much less well appreciated, but equally important, issue of stability in the presence of contaminants. The adsorption behavior of this material toward various gases is under investigation, with predicted hydrogen uptake from simulation being comparable to those of record-holding materials.

■ ASSOCIATED CONTENT

Supporting Information

Detailed procedure for simulation, synthesis of ligands and MOFs, activation procedure of MOFs, single crystal data, PXRD pattern, TGA, DRIFTS, and detailed BET calculation. This material is available free of charge via the Internet at http://pubs.acs.org

■ AUTHOR INFORMATION

Corresponding Authors

*o-farha@northwestern.edu
*j-hupp@northwestern
*stoddart@northwestern.edu
*snurr@northwestern.edu

Author Contributions

⊥These authors contributed equally.

Notes

The authors declare no competing financial interest.

■ ACKNOWLEDGMENTS

O.K.F., R.Q.S., and J.T.H.: This work (modeling, MOF assembly and experimental characterization) was supported as part of the Inorganometallic Catalyst Design Center, an Energy Frontier Research Center, funded by the U.S. Department of Energy, Office of Science, Basic Energy Sciences, under Award DESC0012702. J.F.S: This research is part (Project 34-944) of the Joint Center of Excellence in Integrated Nano-Systems (JCIN) at King Abdulaziz City for Science and Technology (KACST) and Northwestern University (NU). The authors would like to thank both KACST and NU for their continued support of this research.

■ REFERENCES

(1) O'Keeffe, M.; Peskov, M. A.; Ramsden, S. J.; Yaghi, O. M. *Acc. Chem. Res.* **2008**, *41*, 1782.
(2) Férey, G. *Chem. Soc. Rev.* **2008**, *37*, 191.
(3) Horike, S.; Shimomura, S.; Kitagawa, S. *Nat. Chem.* **2009**, *1*, 695.
(4) Farha, O. K.; Özgür Yazaydın, A.; Eryazici, I.; Malliakas, C. D.; Hauser, B. G.; Kanatzidis, M. G.; Nguyen, S. T.; Snurr, R. Q.; Hupp, J. T. *Nat. Chem.* **2010**, *2*, 944.
(5) Furukawa, H.; Ko, N.; Go, Y. B.; Aratani, N.; Choi, S. B.; Choi, E.; Yazaydin, A. Ö.; Snurr, R. Q.; O'Keeffe, M.; Kim, J.; Yaghi, O. M. *Science* **2010**, *329*, 424.
(6) Farha, O. K.; Eryazici, I.; Jeong, N. C.; Hauser, B. G.; Wilmer, C. E.; Sarjeant, A. A.; Snurr, R. Q.; Nguyen, S. T.; Yazaydın, A. Ö.; Hupp, J. T. *J. Am. Chem. Soc.* **2012**, *134*, 15016.
(7) Senkovska, I.; Kaskel, S. *Chem. Commun.* **2014**, *50*, 7089.
(8) Toyota ushers in the future with lauch of the Mirai fuel cell sedan. http://www.toyota-global.com/innovation/environmental_technology/fuelcell_vehicle/ (Accessed December 4, 2014).
(9) Furukawa, H.; Cordova, K. E.; O'Keeffe, M.; Yaghi, O. M. *Science* **2013**, *341*, 974.
(10) Yaghi, O. M.; O'Keeffe, M.; Ockwig, N. W.; Chae, H. K.; Eddaoudi, M.; Kim, J. *Nature* **2003**, *423*, 705.
(11) Stoeck, U.; Krause, S.; Bon, V.; Senkovska, I.; Kaskel, S. *Chem. Commun.* **2012**, *48*, 10841.
(12) Banerjee, R.; Furukawa, H.; Britt, D.; Knobler, C.; O'Keeffe, M.; Yaghi, O. M. *J. Am. Chem. Soc.* **2009**, *131*, 3875.
(13) Biswal, B. P.; Chandra, S.; Kandambeth, S.; Lukose, B.; Heine, T.; Banerjee, R. *J. Am. Chem. Soc.* **2013**, *135*, 5328.
(14) Nelson, A. P.; Farha, O. K.; Mulfort, K. L.; Hupp, J. T. *J. Am. Chem. Soc.* **2008**, *131*, 458.
(15) Farha, O. K.; Hupp, J. T. *Acc. Chem. Res.* **2010**, *43*, 1166.
(16) Mondloch, J. E.; Karagiaridi, O.; Farha, O. K.; Hupp, J. T. *CrystEngComm* **2013**, *15*, 9258.
(17) Hupp, J. T.; Farha, O. K. Activation of Porous MOF Materials. U.S. Patent 20140206531 A1, July 24, 2014.
(18) Schoenecker, P. M.; Carson, C. G.; Jasuja, H.; Flemming, C. J. J.; Walton, K. S. *Ind. Eng. Chem. Res.* **2012**, *51*, 6513.
(19) Montoro, C.; Linares, F.; Quartapelle Procopio, E.; Senkovska, I.; Kaskel, S.; Galli, S.; Masciocchi, N.; Barea, E.; Navarro, J. A. R. *J. Am. Chem. Soc.* **2011**, *133*, 11888.
(20) Park, K. S.; Ni, Z.; Côté, A. P.; Choi, J. Y.; Huang, R.; Uribe-Romo, F. J.; Chae, H. K.; O'Keeffe, M.; Yaghi, O. M. *Proc. Natl. Acad. Sci. U.S.A.* **2006**, *103*, 10186.
(21) ZIFs are based on imidazolate linkers that are too short to produce high surface area, and zinc pyrazolate MOFs based on the **pcu** topology are prone to catenation, which is detrimental for achieving high surface areas.
(22) Cavka, J. H.; Jakobsen, S.; Olsbye, U.; Guillou, N.; Lamberti, C.; Bordiga, S.; Lillerud, K. P. *J. Am. Chem. Soc.* **2008**, *130*, 13850.
(23) Morris, W.; Volosskiy, B.; Demir, S.; Gándara, F.; McGrier, P. L.; Furukawa, H.; Cascio, D.; Stoddart, J. F.; Yaghi, O. M. *Inorg. Chem.* **2012**, *51*, 6443.
(24) Mondloch, J. E.; Katz, M. J.; Planas, N.; Semrouni, D.; Gagliardi, L.; Hupp, J. T.; Farha, O. K. *Chem. Commun.* **2014**, *50*, 8944.
(25) Decoste, J. B.; Peterson, G. W.; Smith, M. W.; Stone, C. A.; Willis, C. R. *J. Am. Chem. Soc.* **2012**, *134*, 1486.
(26) Zhang, W.; Huang, H.; Liu, D.; Yang, Q.; Xiao, Y.; Ma, Q.; Zhong, C. *Microporous Mesoporous Mater.* **2013**, *171*, 118.
(27) Mondloch, J. E.; Bury, W.; Fairen-Jimenez, D.; Kwon, S.; DeMarco, E. J.; Weston, M. H.; Sarjeant, A. A.; Nguyen, S. T.; Stair, P. C.; Snurr, R. Q.; Farha, O. K.; Hupp, J. T. *J. Am. Chem. Soc.* **2013**, *135*, 10294.

DOI: 10.1021/ja512973b
J. Am. Chem. Soc. 2015, 137, 3585−3591

(28) Gutov, O. V.; Bury, W.; Gomez-Gualdron, D. A.; Krungleviciute, V.; Fairen-Jimenez, D.; Mondloch, J. E.; Sarjeant, A. A.; Al-Juaid, S. S.; Snurr, R. Q.; Hupp, J. T.; Yildirim, T.; Farha, O. K. *Chem.—Eur. J.* **2014**, *20*, 12389.
(29) Feng, D.; Chung, W. C.; Wei, Z.; Gu, Z. Y.; Jiang, H. L.; Chen, Y. P.; Darensbourg, D. J.; Zhou, H. C. *J. Am. Chem. Soc.* **2013**, *135*, 17105.
(30) Jiang, H. L.; Feng, D.; Wang, K.; Gu, Z. Y.; Wei, Z.; Chen, Y. P.; Zhou, H. C. *J. Am. Chem. Soc.* **2013**, *135*, 13934.
(31) Nickerl, G.; Leistner, M.; Helten, S.; Bon, V.; Senkovska, I.; Kaskel, S. *Inorg. Chem. Front.* **2014**, *1*, 325.
(32) Jiang, J.; Gándara, F.; Zhang, Y.-B.; Na, K.; Yaghi, O. M.; Klemperer, W. G. *J. Am. Chem. Soc.* **2014**, *136*, 12844.
(33) Furukawa, H.; Gándara, F.; Zhang, Y.-B.; Jiang, J.; Queen, W. L.; Hudson, M. R.; Yaghi, O. M. *J. Am. Chem. Soc.* **2014**, *136*, 4369.
(34) Liu, T.-F.; Feng, D.; Chen, Y.-P.; Zou, L.; Bosch, M.; Yuan, S.; Wei, Z.; Fordham, S.; Wang, K.; Zhou, H.-C. *J. Am. Chem. Soc.* **2015**, *137*, 413.
(35) Gomez-Gualdron, D. A.; Gutov, O. V.; Krungleviciute, V.; Borah, B.; Mondloch, J. E.; Hupp, J. T.; Yildirim, T.; Farha, O. K.; Snurr, R. Q. *Chem. Mater.* **2014**, *26*, 5632.
(36) Morris, W.; Volosskiy, B.; Demir, S.; Gandara, F.; McGrier, P. L.; Furukawa, H.; Cascio, D.; Stoddart, J. F.; Yaghi, O. M. *Inorg. Chem.* **2012**, *51*, 6443.
(37) Sing, K. S. W.; Everett, D. H.; Haul, R. A. W.; Moscou, L.; Pierotti, R. A.; Rouquerol, J.; Siemieniewska, T. *Pure Appl. Chem.* **1985**, *57*, 603.
(38) Bae, Y.-S.; Yazaydın, A. Ö.; Snurr, R. Q. *Langmuir* **2010**, *26*, 5475.
(39) The fifth peak of the PXRD pattern is systematically more intense in as synthesized samples, which is due to the effect of residual solvent in the framework.
(40) Mondloch, J. E.; Katz, M. J.; Planas, N.; Semrouni, D.; Gagliardi, L.; Hupp, J. T.; Farha, O. K. *Chem. Commun.* **2014**, *50*, 8944.
(41) Suh, M. P.; Park, H. J.; Prasad, T. K.; Lim, D.-W. *Chem. Rev.* **2012**, *112*, 782.
(42) Brunauer, S.; Emmett, P. H.; Teller, E. *J. Am. Chem. Soc.* **1938**, *60*, 309.
(43) Rouquerol, J.; Rouquerol, F.; Llewellyn, P.; Maurin, G.; Sing, K. S. W. *Adsorption by Powders and Porous Solids: Principles, Methodology and Applications*; Academic Press: London, 2013.
(44) Rouqerol, J.; Llewellyn, P. L.; Rouquerol, F. In *Studies in Surface Science and Catalysis*; Llewellyn, P. L., Rodriquez-Reinoso, F., Rouquerol, J., Seaton, N., Eds.; Elsevier: Amsterdam, The Netherlands, 2007; Vol. 160, p 49.
(45) The ratio of BET area to geometric surface area for **NU-1103** is 1.16.

DOI: 10.1021/ja512973b
J. Am. Chem. Soc. 2015, 137, 3585−3591